Theoretical Study of Reactions in the Multiple Well H_2/S_2 System

Chenlai (Ryan) Zhou, Karina Sendt,* and Brian S. Haynes

School of Chemical and Biomolecular Engineering, University of Sydney, 2006 Australia

Received: April 7, 2009; Revised Manuscript Received: May 20, 2009

The potential energy surface of the H_2/S_2 system has been characterized at the full valence MRCI+Davidson/aug-cc-pV(Q+*d*)Z level of theory using geometries optimized at the MRCI/aug-cc-pVTZ level. The analysis includes channels occurring entirely on either the singlet or the triplet surface as well as those involving an intersystem crossing. RRKM-based multiple well calculations allow the prediction of rate constants in the temperature range of 300−2000 K between 0.1 and 10 bar. Of the SH recombined on the singlet surface, the stabilization of the rovibrationally excited adduct HSSH is at the low-pressure limit at 1 bar, but it has a rate comparable to that forming another major set of products $H_2S + S$ (via an intersystem crossing) at temperatures below 1000 K; at higher temperatures, HSS + H becomes the dominant product. For the reaction $H_2S + S$, the presence of an intersystem crossing allows the formation of the singlet excited adduct H_2SS, most of which rearranges and stabilizes as HSSH under atmospheric conditions. At high temperatures, the majority of excited HSSH dissociates to SH + SH and HSS + H. Compared to reported shock tube measurements of the reaction $H_2S + S$, most of the S atom consumption can be described by the triplet abstraction route $H_2S + S \rightarrow SH + SH$, especially at high temperatures, but inclusion of the singlet insertion channel provides a better description of the experimental data. The reaction HSS + H was found to proceed predominantly on the singlet surface without a chemical barrier. The formation of the major product channel SH + SH is very fast at room temperature ($\sim 4 \times 10^{15}$ cm^3 mol^{-1} s^{-1}). While the formation of $H_2S + S$ or $S_2 + H_2$ via an isomerization or an intersystem crossing, respectively, are minor product channels, their rates are significantly higher than those of the corresponding direct triplet channels, except at elevated temperatures. Finally, due to the relatively shallow nature of its well, the stabilization of H_2SS is negligible under conditions of likely interest.

1. Introduction

The self reaction of SH radicals plays an important role in the mechanisms of thermolysis[1] and combustion[2] of H_2S

$$SH + SH \rightarrow \text{products} \quad \text{(R1)}$$

$$\rightarrow HSSH \qquad \Delta H_{0K} = -262 \text{ kJ mol}^{-1} \quad \text{(R1a)}$$

$$\rightarrow H_2SS \qquad \Delta H_{0K} = -147 \text{ kJ mol}^{-1} \quad \text{(R1b)}$$

$$\rightarrow H_2S + S \qquad \Delta H_{0K} = -27 \text{ kJ mol}^{-1} \quad \text{(R1c)}$$

$$\rightarrow HSS + H \qquad \Delta H_{0K} = 43 \text{ kJ mol}^{-1} \quad \text{(R1d)}$$

$$\rightarrow H_2 + S_2 \qquad \Delta H_{0K} = -155 \text{ kJ mol}^{-1} \quad \text{(R1e)}$$

Channel R1a is a significant radical sink responsible for chain termination, while the channels R1a and R1d contribute to the formation of S−S bonds. These channels compete, in particular, with channel R1c, which we showed recently occurs both on the triplet surface, with a small barrier, and via an intersystem crossing, without any barrier.[3] Accurate estimates of reaction rates in the H_2/S_2 system are therefore needed for the modeling of the kinetics of oxidation and thermolysis of H_2S and of the behavior of sulfur species in combustion generally.

Among the various reactions, only the reverse rate of reaction R1c has been determined experimentally[4] and theoretically at a high level.[3] In earlier work, our group[1] estimated the reverse rate reaction R1a via an RRKM master equation method, but as noted by Cerru et al.,[2] that result coupled with the experimental equilibrium constant gives rise to unusual temperature dependence. We attribute this to the inconsistency in the heat of reaction R1a between the G2 energy (used to derive the rate constant) and standard thermochemical data (used for computing the equilibrium constant), noting that the enthalpy of formation for SH has been revised by a few kJ mol^{-1} recently.[5] We[1] also estimated the forward and reverse rates of reaction R1d using the quantum RRK (QRRK) approach to ascertain what fraction of the intermediate adduct HSSH* would stabilize; however, we did not include the possibility that HSSH* might form $H_2S + S$, H_2SS, or $H_2 + S_2$, which the more recent PES[3] has revealed can arise from the chemically activated species and an intersystem crossing.

It is apparent that a comprehensive treatment of the multiple product channels on the H_2/S_2 surface is essential to determining the kinetics of the various reactions. This paper presents our work on this topic using the PES characterized at high levels of theory. We employ RRKM-based multiple well calculations to determine kinetic parameters as functions of both temperature and pressure for channels important to both atmospheric and combustion modeling with N_2 as the bath gas.

* To whom correspondence should be addressed. E-mail: k.sendt@usyd.edu.au.

10.1021/jp903185k CCC: $40.75
Published on Web 07/01/2009

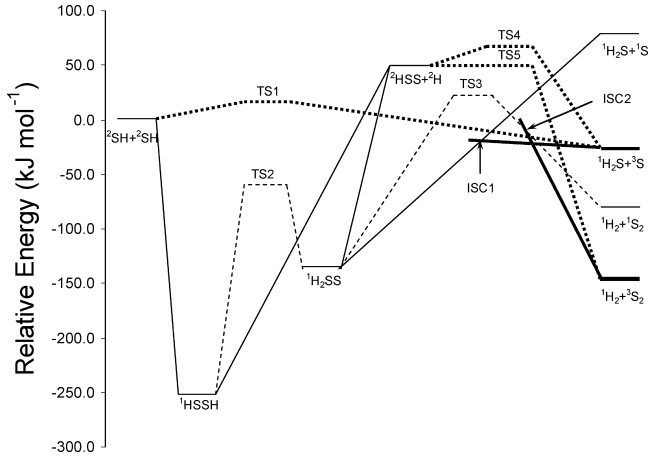

Figure 1. Potential energy diagram for the H_2/S_2 system characterized at the full valence MRCI+Davidson/aug-cc-pV(Q+*d*)Z level of theory with geometries at the MRCI/aug-cc-pVTZ level and ZPVE at the CASSCF/aug-cc-pVTZ in previous[3] and this work; thick lines, triplet surface; thin lines, singlet surface. The transition state connecting HSSH and $S_2 + H_2$ is not shown due to the very high barrier.

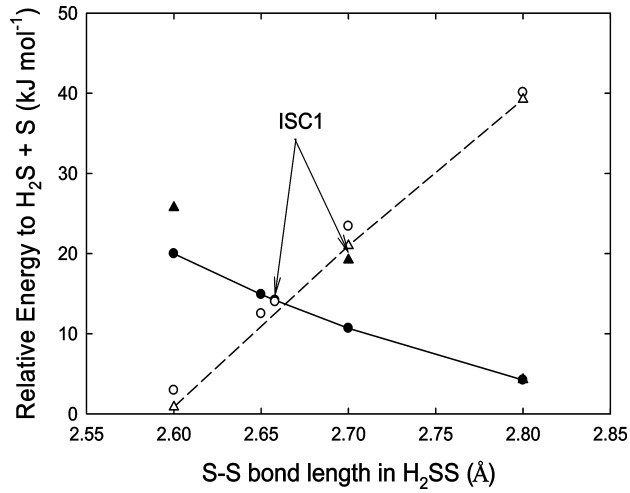

Figure 2. The slice of the PES characterized at the MRCI/aug-cc-pVTZ level, indicating the occurrence of ISC1 for R6; solid circles, triplet energies at triplet geometries; open circles, singlet energies at triplet geometries; solid triangles, triplet energies at singlet geometries; open triangles, singlet energies at singlet geometries; solid lines, optimized triplet surface; broken lines, optimized singlet surface.

2. Computational Methods

2.1. Characterizing the Potential Energy Surface. As shown in the PES in Figure 1, the unimolecular channels found to proceed entirely on the singlet surface are

$$HSSH \rightarrow SH + SH \quad (R2)$$

$$HSSH \rightarrow HSS + H \quad (R3)$$

$$HSSH \rightarrow H_2SS \quad (R4)$$

$$H_2SS \rightarrow HSS + H \quad (R5)$$

In addition, the intersystem crossings ISC1 and ISC2 allow the formation of triplet $H_2S + S$ and $S_2 + H_2$, respectively, via the unimolecular dissociation of singlet H_2SS

$$H_2SS \rightarrow H_2S + {}^3S \quad (R6)$$

$$H_2SS \rightarrow {}^3S_2 + H_2 \quad (R7)$$

In the H_2/S_2 system, we have for completeness considered other elementary channels that may occur entirely on the triplet surface

$$SH + SH \rightarrow H_2S + S \quad (R8)$$

$$HSS + H \rightarrow H_2S + S \quad (R9)$$

$$HSS + H \rightarrow S_2 + H_2 \quad (R10)$$

It should be noted however that the sulfur abstraction channel −R1d via a saddle point on the triplet surface was not included in this work as its rate is significantly lower than that of singlet reaction −R1d.[1]

For channels occurring entirely on the singlet or triplet surface, consistency with the previous theoretical study of the H_2/S_2 system[3] was achieved by characterizing the ground-state surfaces using multiconfigurational methods with full valence active space. The geometry, energy, and vibrational frequencies of TS1 and TS2 were adopted directly from previous work,[3] while additional calculations were performed for the transition states of the remaining channels. These transition-state geometries are all at the MRCI/aug-cc-pVTZ level of theory. Subsequent single-point energy calculations were performed at the MRCI/aug-cc-pV(Q+*d*)Z level with the Davidson correction. The corresponding vibrational frequencies and zero-point vibrational energy corrections (ZPVE) were calculated at the CASSCF/aug-cc-pVTZ level using CASSCF geometries (unless otherwise noted). In an effort to characterize the slice of the PES for the unimolecular dissociation channels (reactions R2, R3, and R5), the geometries of the relevant transition states were determined by performing partial optimizations at the MRCI/aug-cc-pVTZ level of theory with one bond length being constrained at a range of values representing the reaction coordinate.

For reactions involving an intersystem crossing, the transition state was chosen to be the higher of the lowest point at which surface crossing occurs or the saddle point over which the reaction proceeds. The PES shown in Figure 1 indicates that the transition state of the reaction R6 occurs at the crossing point ISC1. According to the two-dimensional PES in our earlier work,[3] the lowest intersystem crossing point for the channel R6 is expected to occur in the regime where the S−S bond of H_2SS is stretched to 2.6−2.8 Å. In an effort to determine the geometry at the crossing point, trial partial optimizations were performed at the MRCI/aug-cc-pVTZ level of theory on both the singlet and triplet ground surface with the frozen S−S bond length lying in the range from 2.6 to 2.8 Å. Additional single-point energies were calculated at the same level of theory to produce the triplet energies at the geometry optimized on the singlet surface and vice versa as shown in Figure 2. From the one-dimensional PES obtained for the reaction coordinate of reaction R6 by stretching the S−S bond of H_2SS, the intersystem crossing point is estimated to lie in the region where the discrepancy between singlet and triplet energies, calculated at the same geometry, is <0.5 kJ mol^{-1}. Using this geometry, the corresponding single-point energy was taken as the average value of singlet and triplet energies at the MRCI+Davidson/

aug-cc-pV(Q+*d*)Z level. For the channel R7, ISC2 is on the product side, and hence, the properties of TS3 determine the kinetic behavior of this reaction.

The quantum chemistry calculations were performed using Molpro[6] and Dalton[7] packages.

2.2. Kinetics. The temperature and pressure dependences for reactions of interest in the H_2/S_2 system were studied by performing RRKM calculations using the Multiwell program suite.[8] The normal modes representing the torsional and rocking motions in the loose transition state were treated as one-dimensional and two-dimensional internal rotations, respectively, while the extremely hindered internal rotors were treated as harmonic oscillators. The solid angle representing the extent of the steric hindrance of the rocking motions was calculated using the GEOM package in the UNIMOL program suite.[9] The transition states for barrierless channels were identified variationally by minimizing the temperature-dependent high-pressure rate constants. Along with TS2 and TS3, these were then used to generate the microcanonical rate constant $k(E)$ using Multiwell.

In order to estimate the rate of channel R6, which proceeds via intersystem crossing, we must adjust the rate constants $k(E)$ (calculated at the crossing point) by a factor to account for the crossing efficiency. Here, we used the factor 0.2, which we earlier found as the average value of the ratio of the fitted pre-exponential factor for the sulfur insertion channel ($H_2S + S$)[3] to its Lennard-Jones collision frequency in the temperature range of 300−2000 K. While taking this approach is somewhat speculative, it does allow us to estimate the possible role of reaction R6 in the multiple well system.

The Lennard-Jones collision parameters for N_2 were taken from Hippler et al.,[10] while those for HSSH and H_2SS were estimated according to empirical formulas[11] using the boiling temperature of HSSH (343.85 K).[12] In order to describe the collisional energy transfer in the H_2/S_2 system, an exponential down model[13] was employed, with the temperature-independent $\langle\Delta E_{down}\rangle$ value of 230 cm^{-1} taken from the literature for N_2 as the collider in the similar-sized HSO_2 system.[14] According to the approximate expressions (eqs E1 and E2) proposed by Hippler et al.[10] and Troe,[15] respectively, this $\langle\Delta E_{down}\rangle$ value corresponds to a $\langle\Delta E\rangle$ value of -121 cm^{-1} and a collision efficiency (β_c) of 0.5 at 300 K (F_E assumed to be 1.0)

$$-\langle\Delta E\rangle \approx \frac{\langle E_{down}\rangle^2}{\langle E_{down}\rangle + kT} \quad \text{(E1)}$$

$$\frac{\beta_c}{1-\sqrt{\beta_c}} \approx \frac{-\langle\Delta E\rangle}{F_E kT} \quad \text{(E2)}$$

Given the lack of reliable parameters describing the collisional energy transfer in the H_2/S_2 system, we assessed the sensitivity of the Multiwell rate constants to the $\langle\Delta E_{down}\rangle$ value. As expected, channels leading to the unimolecular product (HSSH or H_2SS) are most affected by the variation of the $\langle\Delta E_{down}\rangle$ value, showing near-first-order dependence. Nevertheless, the uncertainty in the collisional energy transfer becomes negligible at higher temperatures when collisional stabilization is less important.

In the Multiwell simulations of the reactions in the H_2/S_2 system, bimolecular reactants of interest were allowed to form the chemically activated adduct, and the product distributions were calculated in the temperature range of 300−2000 K between 0.1 and 10 bar (unless otherwise noted). The effect of tunneling was not considered even for the channels with a substantial barrier (reactions R4 and R7). An estimate using Wigner's formulation[16] shows that neglecting the effect of tunneling introduces error factors of ∼2.1 (reaction R4) and ∼3.6 (reaction R7) at 300 K, reducing to ∼1.1 and ∼1.2 at 1000 K, respectively. In order to assess the significance of such errors, we carried out trial calculations at 300 K in which $k(E)$ was scaled artificially by factors of 2 for reaction R4 and 4 for reaction R7. These calculations showed that no significant changes occurred in the rates of the major channels, and it is concluded that our results overall are insensitive to the neglect of tunneling in reactions R4 and R7.

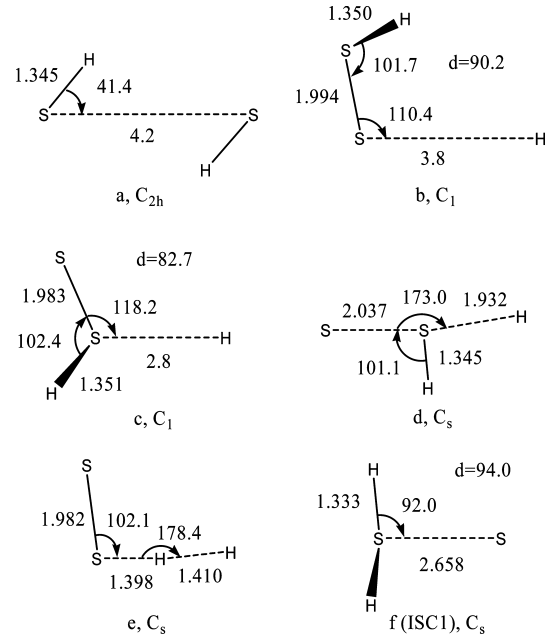

Figure 3. Geometry parameters of transition states in the singlet unimolecular channels (a) R2, (b) R3, and (c) R5 at 1000 K, triplet channels (d) R9 and (e) R10, and the intersystem crossing point (f) in reaction R6. Bond lengths and angles are given in Å and degrees, respectively.

The rate constants for bimolecular channels on the triplet surface (reactions R9 and R10) were simply evaluated by transition-state theory (TST) with vibrational partition functions computed using the harmonic oscillator assumption. The tunneling contribution was estimated according to Wigner's formulation.[16]

The rate constants for channels of interest were fitted to a three-parameter Arrhenius expression using a least-squares method.

3. Results and Discussion

3.1. The Potential Energy Surface. Geometry parameters for the transition states and the intersystem crossing point studied in this work are presented in Figure 3. As the channels proceeding via saddle points TS1−TS3 have been discussed in detail previously,[3] we focus here on the PES relevant to the unimolecular dissociation channels R2, R3, R5, and R6 on the singlet surface and bimolecular channels R9 and R10 on the triplet surface. Given an estimated uncertainty of ∼10 kJ mol^{-1} in the current computational methods,[3] the MRCI energies for channels R2 and R3 were scaled to give the heats of reaction, in line with the values at 0 K extrapolated from experimental values for $\Delta H^\circ_{f,298}$ summarized in our earlier work.[3] The relative energies for channels R5 and R6 were not scaled due to the lack of experimental data for $\Delta H^\circ_{f,298}$ (H_2SS).

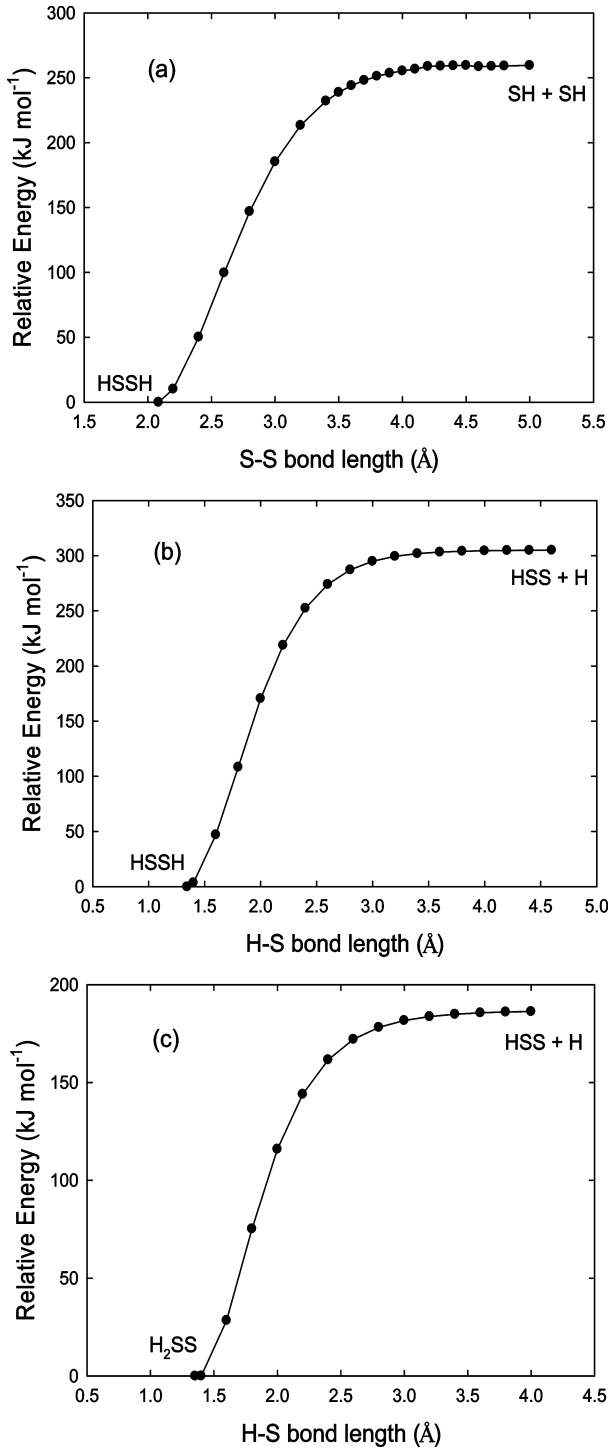

Figure 4. The slice of the PES for reaction (a) R2, (b) R3, and (c) R5 characterized at the MRCI+Davidson/aug-cc-pV(Q+*d*)Z level using geometries partially optimized at the MRCI/aug-cc-pVTZ level and ZPVE calculated at the CASSCF/aug-cc-pVTZ level. For reaction R2 at the S−S separation of 4.2−4.5 Å, ZPVE was calculated at the MRCI/aug-cc-pVTZ level. Additional scaling is applied to reactions R2 and R3 in order obtain heats of reaction consistent with the thermal data (see text).

Panels (a), (b), and (c) in Figure 4 represent the slices of the PES for the bond fission channels R2, R3, and R5, respectively. It is clear that the cleavage of each of these bonds is barrierless beyond the endothermicity of the reaction. The loose transition states minimizing the high-pressure limit rate coefficients for these channels were identified at the points on the PES where the breaking bonds were extended to about twice the corresponding equilibrium length.

In stretching the S−S bond in the channel R2, the geometry of the loose transition state shifts from staggered to trans-planar at the S−S separation of 4.2 Å; see Figure 3. With this change, the H−S−S angle becomes significantly smaller, going from ∼80° at 4.1 Å to ∼40° at 4.2 Å. Consequently, while the rocking motions of the SH moieties are found to be unhindered for S−S separations in the range of 3.2−4.1 Å, steric hindrance is appreciable beyond that, with a hindrance angle of 85° at 4.2 Å rising to 145° at 4.5 Å. Since the CASSCF geometries still remain staggered until further stretching to 4.6 Å, the apparent difference between the CASSCF and MRCI geometries of the loose transition state at the S−S separations in the range of 4.2−4.5 Å introduces uncertainties in computing the vibrational frequencies and ZPVE. Therefore, these quantities were calculated numerically at the MRCI/aug-cc-pVTZ level of theory using the partially optimized MRCI geometries. It was found that the ZPVE calculated at the staggered CASSCF geometries was ∼2 kJ mol^{-1} lower than those using planar MRCI geometries. While the discrepancy of this magnitude is well within the uncertainty of the method, it leads to an increase of the rate coefficient of reaction R2 by a factor of 2 at 300 K, becoming negligible at temperatures above 1000 K.

For the channel R6 shown in Figure 2, the lowest intersystem crossing energy was found at the MRCI geometry with an S−S separation of 2.658 Å. While the discrepancy between the singlet and triplet energies is only 0.2 kJ mol^{-1} at the MRCI/aug-cc-pVTZ level, it increases slightly to 2 kJ mol^{-1} at the MRCI + Davidson/aug-cc-pV(Q+*d*)Z level. The intersystem crossing energy of −25 kJ mol^{-1} (calculated as the average value of singlet and triplet energies, excluding ZPVE corrections) relative to the asymptote SH + SH is in good agreement with the lowest crossing energy (∼−20 kJ mol^{-1}) determined from the contour plots of the two-dimensional PES for the H_2/S_2 system.[3] The relaxation of more degrees of freedom in the partial optimizations is responsible for the somewhat lower and also more accurate crossing energy obtained in this work. The vibrational frequencies and ZPVE for the intersystem crossing point were calculated by performing partial optimizations at the CASSCF/aug-cc-pVTZ level. The S−S bond length is constrained at the value corresponding to the geometry at the intersystem crossing point. It was found that the discrepancy between the CASSCF and MRCI geometry parameters is less than 3%, suggesting that the geometry is insensitive to the level of the multiconfigurational method in the H_2/S_2 system. Since triplet H_2SS is not stable, the reaction $H_2S + S \rightarrow H_2SS$ is prohibited on the triplet surface, leading to the absence of imaginary frequency for the triplet intersystem crossing point. Thus, we use the frequencies and ZPVE calculated on the singlet surface. Taking the intersystem crossing point as the transition state, we obtain a barrier height of ∼14 kJ mol^{-1} for the channel −R6.

On the triplet surface, the barrier heights of channels R9 and R10 are in reasonable agreement with those characterized previously at the G2 level using CASSCF geometries.[1] In this work, a relatively lower but still significant barrier was found for reaction R9 at the MRCI level (∼15 versus ∼26 kJ mol^{-1}). For the abstraction channel R10, the barrier was confirmed to be very small, ∼0.5 kJ mol^{-1}.

3.2. Kinetics. In deriving the high-pressure rate constant for reaction R2, the low vibrational frequencies of the loose transition state with the trans-planar structure were treated as two types of internal rotations, rocking and torsional motions. The rocking motions corresponding to vibrational frequencies

TABLE 1: High-Pressure Rate Constants and Equilibrium Constants for the Unimolecular Channels in the H_2/S_2 System

	rate parameters (cm, s, kJ, mol, K units)			equilibrium constants (cm, kJ, mol, K units)[a]		
reaction	*A*	*n*	*E*	*A*	*n*	*E*
R2: HSSH = SH + SH	1.59×10^{18}	–0.957	267	4.61×10^{5}	–1.112	273
R3: HSSH = HSS + H	4.70×10^{17}	–0.076	310	3.71×10^{2}	–0.476	310
R4: HSSH = H_2SS	6.74×10^{12}	0.213	193	2.18×10^{0}	–0.166	116
R5: H_2SS = HSS + H	1.46×10^{15}	–0.026	191	1.70×10^{2}	–0.311	195
R6: H_2SS = H_2S + S	4.53×10^{11}	0.468	127	1.59×10^{4}	–0.923	127
R7: H_2SS = S_2 + H_2	1.36×10^{10}	1.125	158	7.66×10^{2}	–0.706	–1

[a] Calculated using NIST thermochemical Tables[18] for H, H_2, S, S_2, and H_2S with other literature $\Delta H^{\circ}_{f,298}$ for SH, HSS, HSSH, and H_2SS summarized in Zhou et al.[3]

TABLE 2: Rate Constants Derived from Multiwell Simulations and TST

		rate parameters (cm, s, kJ, mol, K units)			Troe parameters		
reaction		*A*	*n*	*E*	α	*T****	*T**
SH + SH + M = HSSH + M[a]	(R1a)	2.33×10^{31}	–4.943	8	1	254	2373
SH + SH = H_2S + S[b]	(R1c)	5.83×10^{16}	–1.763	–4			
H_2S + S + M = HSSH + M[c]		7.43×10^{34}	–5.987	18	72	249	254
HSS + H = SH + SH[b]	(–R1d)	1.63×10^{18}	–0.983	1			
HSS + H = H_2S + S[b]		4.19×10^{18}	–1.563	2			
HSS + H = H_2S + S[d]	(R9)	1.50×10^{8}	1.551	9			
HSS + H = S_2 + H_2[b]		2.91×10^{16}	–0.894	0			
HSS + H = S_2 + H_2[d]	(R10)	1.05×10^{8}	1.750	–4			

[a] Low-pressure rate constant with N_2 as the bath gas in the temperature range of 300−2000 K; Troe parameters fitted in the pressure range of 0.1−10 bar (Multiwell). [b] Rate constant calculated in the temperature range of 300−2000 K at 1 bar (Multiwell). Rate constants of channel R1c at other pressures are available in the Supporting Information. [c] Low-pressure rate constant with N_2 as the bath gas in the temperature range of 300−1000 K; Troe parameters fitted in the pressure range from 1×10^{-4} to 10 bar (Multiwell). [d] Rate constant calculated in the temperature range of 300−2000 K (TST).

of 50 and 218 cm^{-1} (at 1000 K) were found to be sterically hindered. We therefore treated the two oscillators as a single two-dimensional hindered rotor in computing the rate constant. Treating this sterically hindered rocking motion as a free rotation only increased the rate constant by a factor of 2.2, indicating that there is in fact weak steric hindrance in the loose transition state of reaction R2. Thus, we may deduce that steric hindrance in the torsional motion is also weak and hence treat the torsional vibration (58 cm^{-1} at 1000 K) simply as a free internal rotor in order to avoid the complexity of having to approximate the density of states of the hindered torsional rotor. While this simplification could conceivably lead to overestimation of the rate constants of reaction R2 at low temperatures, the error is expected to become negligible at combustion temperatures.

For the loose transition state in reaction R3, the rocking motions are unhindered, and the two lowest-frequency oscillators are again treated as a two-dimensional free rotor. On the other hand, these motions are severely hindered in reaction R5 and are treated as vibrations.

Table 1 summarizes the high-pressure rate constants for the unimolecular channels R2−R7 along with corresponding equilibrium constants used for the calculation of the reverse rate constants.

In order to understand the effect of multiple channels on the behavior of the product distributions as a function of temperature and pressure for reactions in the H_2/S_2 system, RRKM-based multiple well calculations were performed to reveal the kinetics of the reactions SH + SH, H_2S + S, and HSS + H. These channels are linked by two wells (HSSH and H_2SS) via reaction R2−R7, as shown in Figure 1. The bimolecular channels occurring entirely on the triplet surface do not pass through these wells. Consequently, they were not considered as part of the multiple well system, and hence, they were described separately using the kinetic parameters reported previously (reaction R8)[3] and derived in this work (reactions R9 and R10). Due to the presence of a substantial barrier via TS3 for reaction −R7, the formation of any products from the reaction S_2 + H_2 is expected to be negligibly slow under conditions of interest and was not studied.

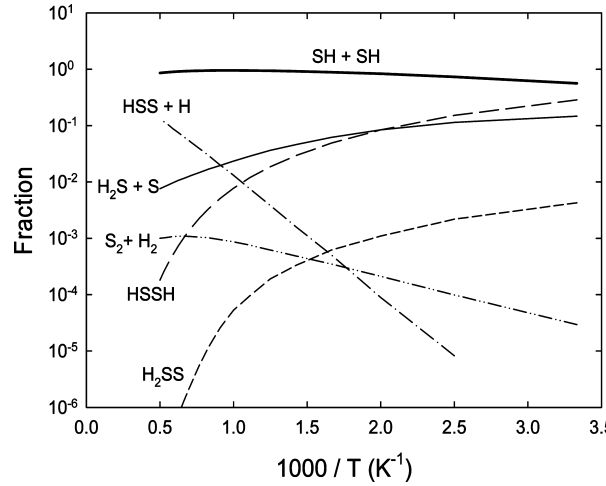

Figure 5. The fate of HSSH* in the reaction SH + SH at 1 bar.

Table 2 presents the kinetic parameters obtained for the bimolecular reactions, as discussed in the following sections.

3.2.1. The Reaction SH + SH. According to the PES shown in Figure 1, the recombination of two SH radicals can form a rovibrationally excited HSSH (HSSH*) at an energy above that of H_2S + S but below that of HSS + H and TS3 (which leads to S_2 + H_2). Figure 5 shows the simulated product distribution for the reaction SH + SH in N_2 at 1 bar. More than 50% of the chemically activated HSSH* reverts to the reactants SH + SH. The formation of H_2S + S occurs upon isomerization of HSSH* to H_2SS*, followed by dissociation after an intersystem crossing. While the rate constant for the stabilization of HSSH is at the low-pressure limit and decreases with the increasing temperature,

it has a value comparable to that for the formation of $H_2S + S$ at temperatures up to 1000 K. At higher temperatures, decomposition of HSSH* to HSS + H becomes competitive and is one order of magnitude faster than the formation of $H_2S + S$ at temperatures above 1800 K. The reaction fluxes forming stable H_2SS or $S_2 + H_2$ from SH + SH are negligible. At higher pressures (5−10 bar), the stabilization of HSSH occurs in the falloff regime at room temperature and becomes the dominant reaction flux for the consumption of HSSH*. However, the product distribution for other channels remains qualitatively similar to that at 1 bar.

Table 2 presents the kinetic parameters for the recombination channel R1a at the low-pressure limit. The unphysical temperature dependence inherent in earlier expressions for the rate of this reaction is now absent. Given that the stabilization of HSSH is in the falloff regime at 10 bar, the rate constants were fitted to a Troe factorization model,[17] yielding parameters ready for the input to a kinetic modeling program such as Chemkin. The high-pressure rate constant is best computed from the reverse rate constant (reaction R2) and the corresponding equilibrium constant reported in Table 1.

The chemically activated bimolecular channel R1c forming $H_2S + S$ is found to be pressure-dependent due to the occurrence of significant stabilization of HSSH at high pressures and low temperatures. The difference between the rate constants of channel R1c at 0.1 and 10 bar is a factor of ∼5 at 300 K, decreasing to ∼1.5 at 600 K. The kinetic parameters reported in Table 2 were computed at 1 bar and should be adjusted by an appropriate factor at high pressures, especially at lower temperatures. We have not investigated this in more detail because the effect is minor at high temperatures. Here, it should also be noted that any deviation of the crossing efficiency from its assumed value of 20% will add to the uncertainty in the values in Table 2.

While the rate constant for the product channel R1d is essentially independent of pressure under the conditions examined, it does have a strong temperature dependence due to the reaction endothermicity. The increase of the reaction flux to HSS + H with the increasing temperature is responsible for the negative temperature dependence for channel R1c. Since reaction R1d is a minor channel at low temperatures, the kinetics are more reliably obtained from the reverse reaction (−R1d) discussed in detail below.

3.2.2. The Reaction $H_2S + S$. When $H_2S + S$ reacts to form H_2SS* via the intersystem crossing ISC1, its subsequent fate is extremely sensitive to both the temperature and the pressure. At pressures above 0.1 bar, the reaction flux mostly passes above TS2, leading to HSSH*, which subsequently either stabilizes as HSSH or dissociates to SH + SH or HSS + H. Consequently, as shown in Figure 6 for the product distribution at 1 bar, the yields of H_2SS and $S_2 + H_2$ are minor.

In the temperature range of 300−500 K, the reaction flux leads predominantly to the stabilization of HSSH. The sulfur insertion reaction $H_2S + S \rightarrow$ HSSH is found to be close to the high-pressure limit even at 1 bar. Since the formation of HSSH is still in the falloff regime at 0.1 bar, Multiwell calculations were extended to lower pressures (down to 1×10^{-4} bar) in order to obtain the low-pressure limit. The presence of the dissociation channels R2 and R3 sees the fraction of HSSH*, which stabilizes, decreasing significantly with increasing temperature (<2% of the total reaction flux, at 1000 K and 1 bar). For this reason, the kinetic parameters reported in Table 2 were fitted only in the temperature range of 300−1000 K.

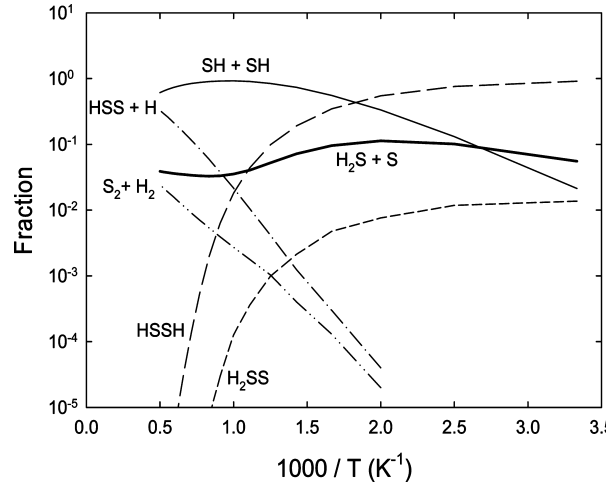

Figure 6. The fate of H_2SS* in the reaction $H_2S + S$ at 1 bar.

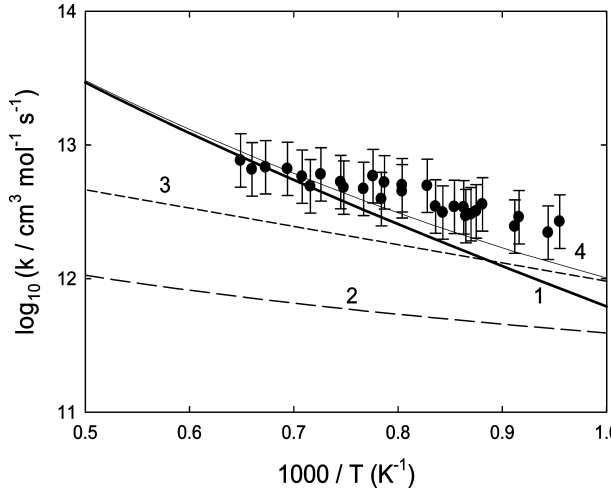

Figure 7. Comparison of the rate constant for $H_2S + S \rightarrow$ products; (1) triplet abstraction channel $H_2S + S \rightarrow SH + SH$ (TST);[3] (2) sulfur insertion channel $H_2S + S \rightarrow$ products (Multiwell, this work); (3) sulfur insertion channel $H_2S + S \rightarrow$ products (fitted to experiments);[3] (4) sum of the abstraction and insertion channels (this work); (•) shock tube measurements.[4]

At higher temperatures, the channel forming the most stable bimolecular products, SH + SH, dominates the product distribution. The equilibrium constants for reaction R1c as calculated by the thermodynamic values (in Table 1) or the rate constants of both directions in Multiwell simulations agreed to a factor of 2−3 at 1 bar, indicating that self-consistency is achieved in the Multiwell simulations. Since it is only for this channel that reliable rate constants can be calculated in both directions over the temperature range of 300−1000 K from Multiwell simulations, similar comparisons are not provided for other channels, which were found to have a relatively high heat of reaction.

Again, due to the high endothermicity, while no reaction to HSS + H was detected below 500 K, its formation via HSSH* has a rate comparable to that of SH + SH at the highest temperatures simulated (1800−2000 K).

Figure 7 compares the results of the theoretical calculations with experimental measurements of the overall rate of disappearance of S atoms in the shock tube reaction of $H_2S + S$.[4] The theoretical results include the contributions of the triplet abstraction channel via TS1[3] and the singlet insertion channel for which the rate constant was derived as that for the disappearance of the reactants in the present Multiwell calculations. While the abstraction channel accounts for most of the

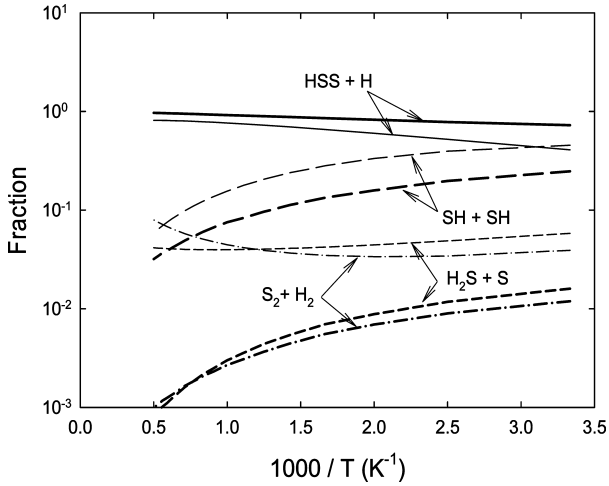

Figure 8. The fate of HSSH* (thick lines) and H_2SS^* (thin lines) in the reaction HSS + H at 1 bar.

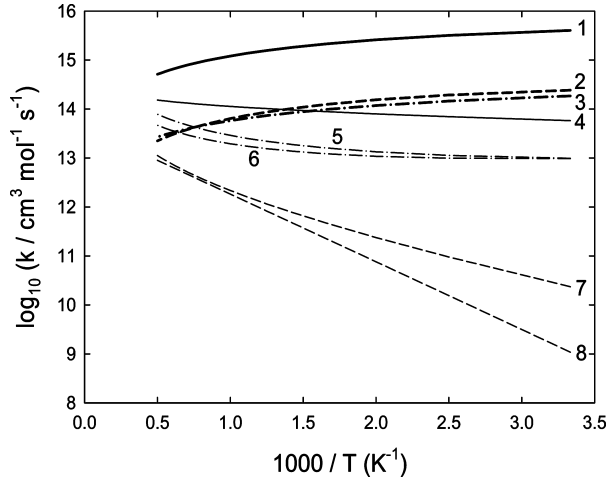

Figure 9. Comparison of rate constants for the reaction HSS + H; (1) HSS + H → SH + SH (Multiwell, this work); (2) HSS + H → H_2S + S (Multiwell, this work); (3) HSS + H → S_2 + H_2 (Multiwell, this work); (4) HSS + H → SH + SH, QRRK;[1] (5) HSS + H → S_2 + H_2, TST (MRCI, this work); (6) HSS + H → S_2 + H_2, TST (CASSCF//G2);[1] (7) HSS + H → H_2S + S, TST (MRCI, this work); (8) HSS + H → H_2S + S, TST (CASSCF//G2).[1]

reaction, the inclusion of the insertion channel yields the better agreement with the measured rate constant in the low-temperature range in particular. In our earlier work on this reaction, we estimated a value of the rate constant for the singlet insertion from the discrepancy between the experimental measurements and the triplet abstraction channel; that value is a factor of ~3.5 higher than the estimate here based on the Multiwell calculations. A difference of this magnitude is well within the combined uncertainties arising from the experiments, the calculation of the rate of the abstraction channel, the Multiwell calculations of the rate of insertion channel, and the estimation of the surface crossing frequency in the insertion rate. The trend of the experimental results suggests a greater role for the insertion channel at lower temperatures, and further experiments under such conditions, preferably with product detection, would provide a more direct estimate for the rate of this channel.

3.2.3. The Reaction of HSS + H. As the stable species with the highest energy in the H_2/S_2 system considered in this work, HSS and H can recombine to access any of the product channels over the temperature range of 300−2000 K. As can be seen from the PES in Figure 1, either HSSH* or H_2SS^* can be formed without any barrier. Although severe steric hindrance in the loose transition state of reaction R5 means that formation of H_2SS^* by reaction −R5 is less likely (by a factor ~10) than is formation of HSSH* via reaction −R3, we have performed Multiwell simulations for both these situations.

According to the product distribution shown in Figure 8, when HSS + H reacts to form HSSH*, most of this reverts to reactants. The formation of SH + SH is the dominant product channel, being one order of magnitude faster than the channel forming H_2S + S, which, in turn, is faster than the formation of S_2 + H_2 via isomerization to H_2SS^* and subsequent dissociation. These three channels were found to behave as simple bimolecular reactions with no dependence on pressure due to the negligible stabilization of either HSSH or H_2SS, even at 10 bar.

If the initial reaction forms H_2SS^*, the dissociation back to HSS + H is less likely, corresponding to larger fractional formation of bimolecular products, albeit with a lower overall rate constant. This is attributed to the significantly lower rate constant of channel −R5 than that of channel −R3, as mentioned earlier. Again, no stabilization of either HSSH or H_2SS was detected under the conditions of interest, and the bimolecular product channels were not influenced by pressure.

The rate constants for the formation of SH + SH, H_2S + S, and S_2 + H_2 reported in Table 2 were calculated as the sum of the reaction fluxes via HSSH* and H_2SS^*. Figure 9 compares the reported rate constants[1] of product channels occurring in the reaction HSS + H with the predicted values in this work. For channels R9 and R10, the rate constants derived using the MRCI PES are in good agreement with those at the G2 level, except for reaction R9 at temperatures below 1000 K. The reduction of the barrier height by ~9 kJ mol^{-1} accounts for the fact that the rate constant is higher than that previously predicted at the lower temperatures. On the singlet surface, the reaction HSS + H → SH + SH is significantly faster than that previously predicted in QRRK analysis,[1] especially at low temperatures (70 times faster at 300 K). The use of the more reliable MRCI PES is, in part, responsible for such discrepancy.

While H_2S + S is the minor product channel for the recombination reaction HSS + H, its rate of formation at 300−1000 K is several orders of magnitude faster than that of the triplet bimolecular channel R9, which needs to overcome a barrier height of ~15 kJ mol^{-1}. With a comparable branching ratio to the formation of H_2S + S on the singlet surface, HSS + H → S_2 + H_2 also remains significantly faster than the corresponding triplet hydrogen abstraction route (reaction R10) until elevated temperatures are reached. It should be noted however that the estimated crossing efficiency has a strong influence on the computed rate constant for these minor channels.

4. Conclusions

Multiwell simulations for the reactions SH + SH and H_2S + S show that the stabilization of HSSH is in the falloff regime at low temperatures between 1 and 10 bar, while the formation of the less stable adduct H_2SS is negligible. At high temperatures, of the HSSH* formed, the majority dissociates to SH + SH, while the formation of HSS + H becomes significant at elevated temperatures. The rate constant for the reaction H_2S + S, derived as the sum of the hydrogen abstraction channel (reaction −R8) on the triplet surface and the singlet pathways via an intersystem crossing, is in good agreement with experimental values, revealing that SH + SH is predominantly formed on the triplet surface and the branching ratio for the formation of HSS + H is less than 2% at 1000−2000 K. The reaction HSS + H via singlet HSSH* was found to be barrierless and

very fast at room temperature ($\sim 4 \times 10^{15}$ cm^3 mol^{-1} s^{-1}), mostly leading to SH + SH. Despite the relatively low branching ratio for the formation of H_2S + S and S_2 + H_2, they are significantly faster than the corresponding simple bimolecular routes which proceed entirely on the triplet surface, except for HSS + H → S_2 + H_2 at very high temperatures. Finally, Multiwell simulations indicate that the inclusion of all channels considered in this work is necessary to compute the rate constants over a wide range of conditions. In particular, the possibility of a surface crossing can greatly affect the kinetics of channels related to H_2S + S.

Acknowledgment. The authors acknowledge the support of the Australian Research Council for part of this work. The computations were performed at the Australia Partnership for Advanced Computing (APAC) at the Australian National University, Canberra. Chenlai (Ryan) Zhou thanks the School of Chemical and Biomolecular Engineering of the University of Sydney for the award of the FH Loxton Postgraduate Studentship.

Supporting Information Available: Rate constants for the chemically activated reaction SH + SH → H_2S + S as functions of both temperature and pressure. This material is available free of charge via the Internet at http://pubs.acs.org.

References and Notes

(1) Sendt, K.; Jazbec, M.; Haynes, B. S. *Proc. Combust. Inst.* **2003**, *29*, 2439–2446.

(2) Cerru, F. G.; Kronenburg, A.; Lindstedt, R. P. *Combust. Flame* **2006**, *146*, 437–455.

(3) Zhou, C.; Sendt, K.; Haynes, B. S. *J. Phys. Chem. A* **2008**, *112*, 3239–3247.

(4) Shiina, H.; Oya, M.; Yamashita, K.; Miyoshi, A.; Matsui, H. *J. Phys. Chem.* **1996**, *100*, 2136–2140.

(5) Shiell, R. C.; Hu, X. K.; Hu, Q. J.; Hepburn, J. W. *J. Phys. Chem. A* **2000**, *104*, 4339–4342.

(6) Werner, H. J.; Knowles, P. J.; Lindh, R.; Manby, F. R.; Schütz, M.; Celani, P.; Korona, T.; Rauhut, G.; Amos, R. D.; Bernhardsson, A.; Berning, A.; Cooper, D. L.; Deegan, M. J. O.; Dobbyn, A. J.; Eckert, F.; Hampel, C.; Hetzer, G.; Lloyd, A. W.; Menicholas, S. J.; Meyer, W.; Mura, M. E.; Nicklass, A.; Palmieri, P.; Pitzer, R.; Schumann, U.; Stoll, H.; Stone, A. J.; Tarroni, R.; Thorsteinsson, T. *MOLPRO, a package of ab initio programs*, version 2006.1;2006; http://www.molpro.net.

(7) DALTON, a molecular electronic structure program, Release 2.0; http://www.kjemi.uio.no/software/dalton/dalton.html (2005).

(8) (a) Barker, J. R. *Int. J. Chem. Kinet.* **2001**, *33*, 232–245. (b) MultiWell-2008.2 Software; designed and maintained by Barker, J. R. with contributions from Ortiz, N. F.; Preses, J. M.; Lohr, L. L.; Maranzana, A.; Stimac, P. J. University of Michigan: Ann Arbor, MI, http://aoss.engin.umich.edu/multiwell/ (2008).

(9) Gilbert, R. G.; Smith, S. C.; Jordan, M. J. T. *UNIMOL program suite*, (calculation of fall-off curves for unimolecular and recombination reactions; 1990).

(10) Hippler, H.; Troe, J.; Wendelken, H. J. *J. Chem. Phys.* **1983**, *78*, 6709–6717.

(11) Gilbert, R. G.; Smith, S. C. *Theory of Unimolecular and Recombination Reactions*; Blackwell: Oxford, U.K., 1990.

(12) Lide, D. R.; Baysinger, G.; Kehiaian, H. V.; Berger, L. I.; Kuchitsu, K.; Goldberg, R. N.; Roth, D. L.; Haynes, W. M.; Zwillinger, D. *CRC Handbook of Chemistry and Physics*, 88th ed.; CRC Press: Boca Raton, FL, 2008.

(13) Penner, A. P.; Forst, W. *J. Chem. Phys.* **1977**, *67*, 5296–5307.

(14) Hughes, K. J.; Blitz, M. A.; Pilling, M. J.; Robertson, S. H. *Proc. Combust. Inst.* **2003**, *29*, 2431–2437.

(15) Troe, J. *J. Chem. Phys.* **1977**, *66*, 4758–4775.

(16) Wigner, E. *Z. Phys. Chem.* **1932**, *19*, 203–216.

(17) Gilbert, R. G.; Luther, K.; Troe, J. *Ber. Bunsen-Ges. Physik. Chem.* **1983**, *87*, 169–177.

(18) Chase, M. W. *J. Phys. Chem. Ref. Data* 1998. Monograph No. 9.

JP903185K